

Tunable beam splitting via photorefractive nonlinearity and its applications in chiral waveguide induction and vortex generation

Hechong Chen^{†a,b}, Zihan Liu^{†a,b}, Shengdi Lian^{a,b}, Qingying Quan^{a,b}, Boris A. Malomed^c, Shuobo Li^d, Yong Zhang^{a,b}, Huagang Li^{e,*}, Dongmei Deng^{a,b,*}

^a*School of Information and Optoelectronic Science and Engineering, South China Normal University, Guangzhou 510006, China,*

^b*Guangdong Provincial Key Laboratory of Nanophotonic Functional Materials and Devices, South China Normal University, Guangzhou 510631, China,*

^c*Department of Physical Electronics, School of Electrical Engineering, Faculty of Engineering, Tel Aviv University, Tel Aviv 69978, Israel,*

^d*School of Science, Sun Yat-sen University, Guangzhou 510275, China,*

^e*School of Photoelectric Engineering, Guangdong Polytechnic Normal University, Guangzhou 510665, China,*

Abstract

We report experimental observation and theoretical explanation of novel propagation regimes for optical beams in an artificial nonlinear material with outstanding photorefractive properties. Nondiffractive beams, which keep their shapes invariant in the free space, feature self-splitting from the middle in two separating secondary beams, due to the light-matter interaction. The splitting degree is controlled by means of a phase-pre-modulation method. We propose an application of the self-splitting to the creation of an effectively chiral waveguide and the generation of even-order vortices.

1. Introduction

As the development of the integrated-circuit technology is driving the Moore's law towards its limits [1], the demand for new technology platforms is growing. Photonic devices offer superior characteristics for the design of circuitry, such as low loss, high modulation speeds, the ability to implement multi-channel

*Corresponding author

Email address: lhg_3@sina.com and dmdeng@263.net (Dongmei Deng)

schemes, and others [2, 3, 4]. Material elements used for the construction of advanced photonic setups include photonic crystals [5, 6], metamaterials [7, 8], quantum-limitation materials [9, 10], electro-optic crystals [11], etc. Thus, a relevant direction of experimental and theoretical work is the study of light-matter interactions in these media, which reveal phenomena such as topological photonics [12, 13, 14], the Kerr, Pockels, and higher-order nonlinear effects [15, 16], propagation of structured light in metamaterials [17], etc.

In particular, the nonlinearity represented by the photorefractive effect has drawn much interest. It was first observed in 1966 by Ashin *et al.* [18] as wave-front distortions in a coherent light beam propagating through a Lithium Niobate crystal. Governed by the nonlinear Schrödinger equation [19], coupled to the potential equation derived from the band-transport model proposed by Kukhtarev *et al.* [20], photorefractive crystals offer a highly efficient platform for light modulation, in the reciprocal [21, 22] and real [23, 24, 25, 26] spaces alike. While the model of the photorefractive effect is a well-established one, novel phenomena in this area have been recently demonstrated. In particular, Ma *et al.* observed the effective breakdown of the Newton's third law in photorefractive materials such as the strontium barium niobate (SBN) crystal [27], while Xia *et al.* investigated topological phenomena on this platform [22, 28], Diebel *et al.* produced sinusoidal-shaped spatial solitons [29], and Armijo *et al.* and Schwartz *et al.* studied light propagation in disordered photonic lattices with the photorefractive nonlinearity [30, 31].

Nondiffractive beams, featuring invariance of the energy distribution in the course of the propagation, are geometrically protected by the caustics [32, 33]. Due to their unique robustness and longer Rayleigh range, compared to the traditional Gaussian beams, nondiffractive ones have been proposed for the use in complex-environment communications [34] and laser processing [35]. Recently, many works have used nondiffractive beams in SBN crystals, with the aim to confine light in the course of the long-distance propagation [36]. In Ref. [37], the research of analogous optical superfluid, Bessel beam was used to create an obstacle of a few microns diameter, persisting along the propagation distance

measured in several centimeters.

While the diffraction-free propagation is defined as a linear property, the study of effects of optical nonlinearities on these propagation regimes is a relevant problem too. In this article, we address the nonlinear propagation of nondiffractive beams in a SBN crystal. Due to the inherent energy flow in the anisotropic medium, the nondiffractive beams self-split in two secondary lobes. To enhance the degree of splitting, we use spatial phase modulation. Applications of these phenomena to inducing chiral waveguides and generating even-order vortices are briefly discussed too.

2. The theoretical model and experimental setup

We consider the paraxial light propagation, using the nondiffractive Lommel-Gaussian beam (NLGB) as the input, which is the product of the Lommel function and the Gaussian factor [38]:

$$\psi_{\text{NLGB}}(r, \phi, z = 0) = \text{Ga}(r)d^{-n}U_n(dk_t r \exp(i\phi), k_t r), \quad (1)$$

where (r, ϕ) and z are the polar coordinates and propagation distance, $\text{Ga}(r) = \exp(-r^2/w_0^2)$ is the Gaussian factor with width w_0 , $k = 2\pi/\lambda$ is the wavenumber (λ is the wavelength), $k_t = 2\pi/a$ (a is a real constant) is the transverse component of the wave vector, controlling the scale of the beam, integer n is the quantum number of the orbital angular momentum (OAM), and d is the shape factor taking values $0 < |d| < 1$. Further, U_n is the Lommel function defined as:

$$U_n(s, t) = \sum_{p=0}^{\infty} (-1)^p \left(\frac{s}{t}\right)^{n+2p} J_{n+2p}(t), \quad (2)$$

where J_{n+2p} is the Bessel function of the first kind [39]. Because, as seen in Eq. (2), the Lommel function is a superposition of the Bessel functions of different orders, one may expect that the so constructed NLGB may feature some properties of Bessel beams, including the nondiffractive propagation and

carrying the OAM, as shown below. Next, we define the modified Lommel-Gaussian beam (MLGB), by applying a piecewise-constant modulation profile to it:

$$\psi_{\text{MLGB}} = \begin{cases} \psi_{\text{NLGB}}, & |x| > x_s, \\ -\psi_{\text{NLGB}}, & |x| < x_s \end{cases}, \quad (3)$$

where x_s is the splitting scale.

To investigate the propagation of the NLGBs and MLGBs in the nonlinear medium, we solve the nonlinear Schrödinger equation with the input given by Eqs. (1) or (3) [40]:

$$i \frac{\partial}{\partial z} \psi(x, y, z) + \frac{1}{2k_z} [\nabla_{\perp}^2 + V(I)] \psi(x, y, z) = 0, \quad (4)$$

where ∇_{\perp}^2 is the paraxial-diffraction (transverse Laplace) operator, and $V(I) = -k_z^2 n_e^2 r_{33} E_{\text{sc}}(I)$ is the effective nonlinear potential, k_z represents the longitudinal wavenumber, n_e and r_{33} are, respectively, the extraordinary bulk refractive index and electro-optic coefficient ($n_e = 2.2817$ and $r_{33} = 250 \text{ pm}\cdot\text{V}^{-1}$ for the SBN crystal), and $I = |\psi|^2$ is the intensity of the input field. Space-charge carriers excited by the input light field redistribute inside the crystal and form the space-charge electric field, $E_{\text{sc}}(I) = -\partial\varphi_{\text{sc}}(I)/\partial x$. Due to the photorefractive effect, the corresponding potential $\varphi_{\text{sc}}(I)$ is established across the intensity profile, as determined by equation [41]

$$\nabla_{\perp}^2 \varphi_{\text{sc}} + \nabla_{\perp} \ln(1+I) \cdot \nabla_{\perp} \varphi_{\text{sc}} = E_{\text{ext}} \frac{\partial}{\partial x} \ln(1+I) + \frac{k_B T}{e} \left[\nabla_{\perp}^2 \ln(1+I) + (\nabla_{\perp} \ln(1+I))^2 \right], \quad (5)$$

where k_B is the Boltzmann constant, T the temperature, and e the elementary charge. In this equation, intensity I is scaled by the dark intensity I_d , which arises from the thermal excitation of electrons, and can be measured experimentally. The effect of the dark intensity on the beam dynamics was discussed in Ref. [41].

Figure 1(a) displays the writing and erasing setups used for the investigation

of the NLGB and the MLGB' propagation in the SBN crystal. Emitted by a solid-state laser, the 532 nm Gaussian beam is divided by the beam splitter in two. One of them illuminates the reflective spatial light modulator (Santec SLM-200, 1900×1200 pixels), onto which a computer-generated hologram, containing the phase and amplitude information of the lattice-writing beam, is loaded. Then the extraordinarily polarized beam passes through the $4f$ system (incorporating two lenses with the focal distance $f = 300$ mm and a Fourier filter) and the photorefractive Cerium-doped SBN crystal (SBN: 61, $5 \times 5 \times 15$ mm³). To enhance the light-matter interaction, the crystal is externally biased by electric field $E_{\text{ext}} = 1600$ V·cm⁻¹ along the optical c axis (i.e., along x) [26]. Eventually, the beam is recorded by the CCD camera. Due to the memory effect of the refractive-index change, the written photonic structure has to be erased by white-light illumination. The setup is shown in Fig. 1(b). In this setup, the CCD camera monitors the erasing process via the output intensity pattern.

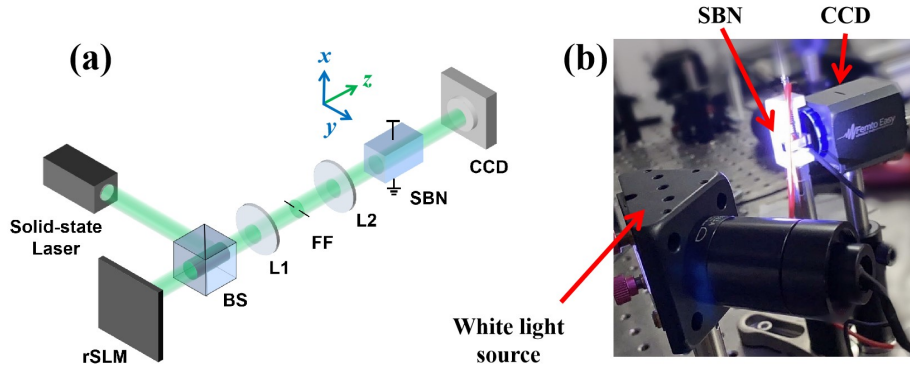


Figure 1: The experimental setups for the investigation of the NLGB and MLGB propagation in the SBN crystal. (a) The schematic of the writing and detecting setups: BS – beam splitter; rSLM – reflective phase-only spatial light modulator; L1 and L2 – lenses with focal length $f = 300$ mm; FF – Fourier filter; CCD – charge-coupled device. (b) The snapshot of the erasing setup.

3. Results and discussions

First, we simulate the propagation of the NLGB in the SBN crystal with parameters $d = 0.9i$, $\lambda = 532$ nm, $w_0 = 0.25$ mm, $a = 0.03$ mm and $n = 1$, under the injection power $P = 4P_0$, $P_0 = 20.3\mu\text{W}$. The intensity and phase distributions in the input plane and the side view of the simulated propagation in the free space are displayed in Figs. 2(a), 2(d) and 2(e), respectively. To quantify the energy flux, we calculate the time-averaged Poynting vector [42]:

$$\langle \vec{S} \rangle = \frac{c_0}{4\pi} \langle \vec{E} \times \vec{B} \rangle = \frac{c_0}{8\pi} [i\omega (\psi \nabla_{\perp} \psi^* - \psi^* \nabla_{\perp} \psi) + 2\omega k |\psi|^2 \vec{e}_z^{\rightarrow}], \quad (6)$$

where c_0 is the light speed in vacuum, \vec{E} and \vec{B} are the electric and the magnetic fields, and ω is the optical frequency. The vectors are indicated by blue arrows in Fig. 2(b). Note that nondiffractive beams with an invariant intensity distribution carry inherent energy flow. However, it is invisible in isotropic media [25], while the situation is different in the SBN crystal with the anisotropic structure. To present the propagation in the crystal, in Fig. 2(f) we display simulated cross sections inside the crystal. The inherent energy flow manifests itself, due to the nonlinearity, at the propagation distance $\simeq 9$ mm. The explanation is that, under the action of the photorefractive effect, electrons excited by the input optical beam drift transversely to the external field and accumulate, resulting in an increase of the refractive index [43]. The so built potential hinders the transverse flux and the energy concentrates in high-intensity spots. On the other hand, the energy is guided towards the direction perpendicular to the electric field, where the space-charge potential is relatively weak, stretching high-intensity spots into two high-energy stripes, as seen in the snapshot at 15 mm in Fig. 2(f). Our experimental result, displayed in Fig. 2(i2) at the back face of the SBN crystal, agrees well with the theoretical prediction. In addition, we also investigate the results under different nonlinearity strengths, controlled by the input power. The simulation and experiments with respect to the intensity distributions are shown in Figs. 2(g) and 2(h). It is seen that the nonlinear strength determines the formation of high-intensity spots and high-

energy stripes.

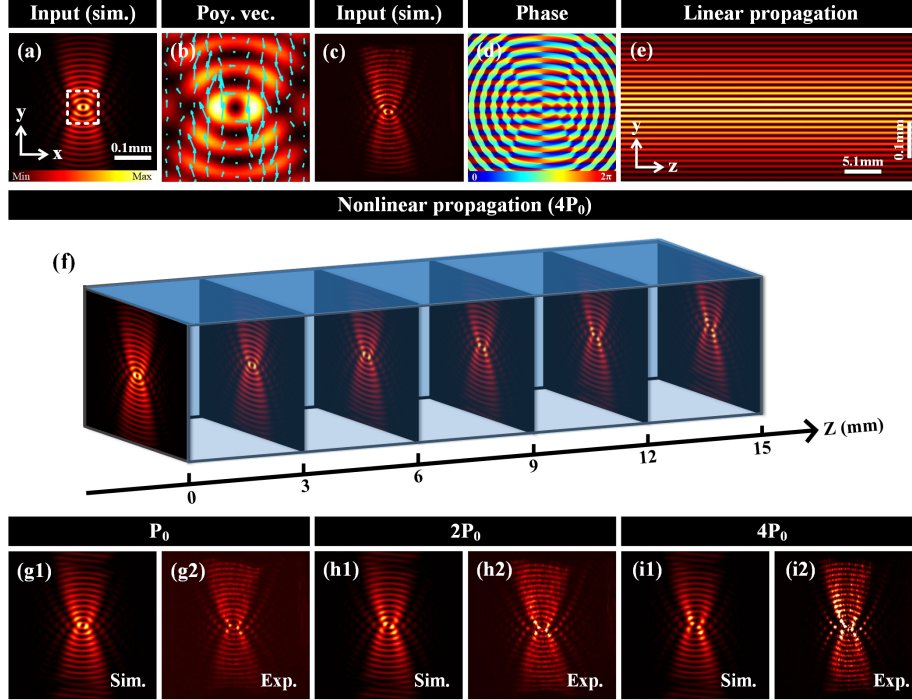


Figure 2: The illustration of the NLGB propagation in the free space and in the photorefractive SBN crystal. (a), (b) and (d) The intensity distribution, Poynting vectors, and phase distribution at the front face of the crystal ($z = 0$), used in the simulations. (c) The experimental result corresponds to (a). (e) Side view of the simulated propagation in the free space. (f) Cross sections of the simulated NLGB propagation in the nonlinear medium with power $P = 4P_0$. (g1), (h1) and (i1) are the simulated output at the back face of the crystal, with powers $P = P_0$, $P = 2P_0$, and $P = 4P_0$, respectively, (g2), (h2) and (i2) being the corresponding experimental snapshots. The parameters are $P_0 = 20.3\mu\text{W}$, $d = 0.9i$, $\lambda = 532\text{ nm}$, $w_0 = 0.25\text{ mm}$, $a = 0.03\text{ mm}$, and $n = 1$.

The numerical and experimental findings reported in Fig. 2 suggest that the NLGB's propagation in the photorefractive crystals leads to self-splitting. To elucidate the physical mechanism of this effect, we analyze the energy flow, energy density and refractive index modulation, as shown in Fig. 3 at different values of the propagation distance. According to the Poynting vectors marked by carmine arrows in Fig. 3(a1), the internal energy flow is predominantly

concentrated on both left and right sides of the beam, being partly distributed transversely, as indicated by the concentration and length of the arrows. Notably, the direction of the Poynting vectors in the left part is down-up, while in the right part it is inverse.

Furthermore, taking into regard the nonlinearly-induced potential redistribution, we present the respective modulation of the local refractive index, calculated according to Refs. [44, 45]:

$$\delta n(I) = -\frac{1}{2}n_e^3 r_{33} E_{sc}(I). \quad (7)$$

The NLGB propagation demonstrates positive feedback in the focusing nonlinear medium. In upper rows of Figs. 3(b1)-3(b6), we show the refractive-index modulation, normalized by the maximum value of the refractive-index change, $\delta n_{\max} = 2.29 \times 10^{-4}$, in the course of the propagation, along left lobes (marked by red dashed lines in the bottom rows) of the NLGB. To quantitatively analyze the nonlinearity, we set value 0.5 as a criterion for it, as indicated by the black dashed line, with the pink and blue regions above and beneath it representing relatively strong and weak modulations, respectively. Indeed, the high-energy central rings and side lobes induce a local increase of the refractive index, indicated by dark-blue and purple patterns in the bottom rows of Figs. 3(b1)-3(b6). In the course of the first 6 mm of the propagation, the central and side peaks rise in the upper rows of Figs. 3(b1)-3(b3). However, only the central peak exceeds 0.5 (from about 0.68 to 1.0), indicating the relatively strong refractive-index modulation. As mentioned above, the self-focusing nonlinearity drives the positive feedback. The energy concentration results in a higher local refractive index, followed by accumulating still more energy at the same spot. The feedback is further observed in the upper row of Figs. 3(b4)-3(b6). The right-side peak, indicated by the black dashed circle, exceeds the 0.5 criterion in Fig. 3(b4) and keeps growing higher. By calculating the peaks in the region of the relatively strong modulation, we find that, in the framework of the displayed picture, the number of peaks increases from 1 to 4, which is a cogent

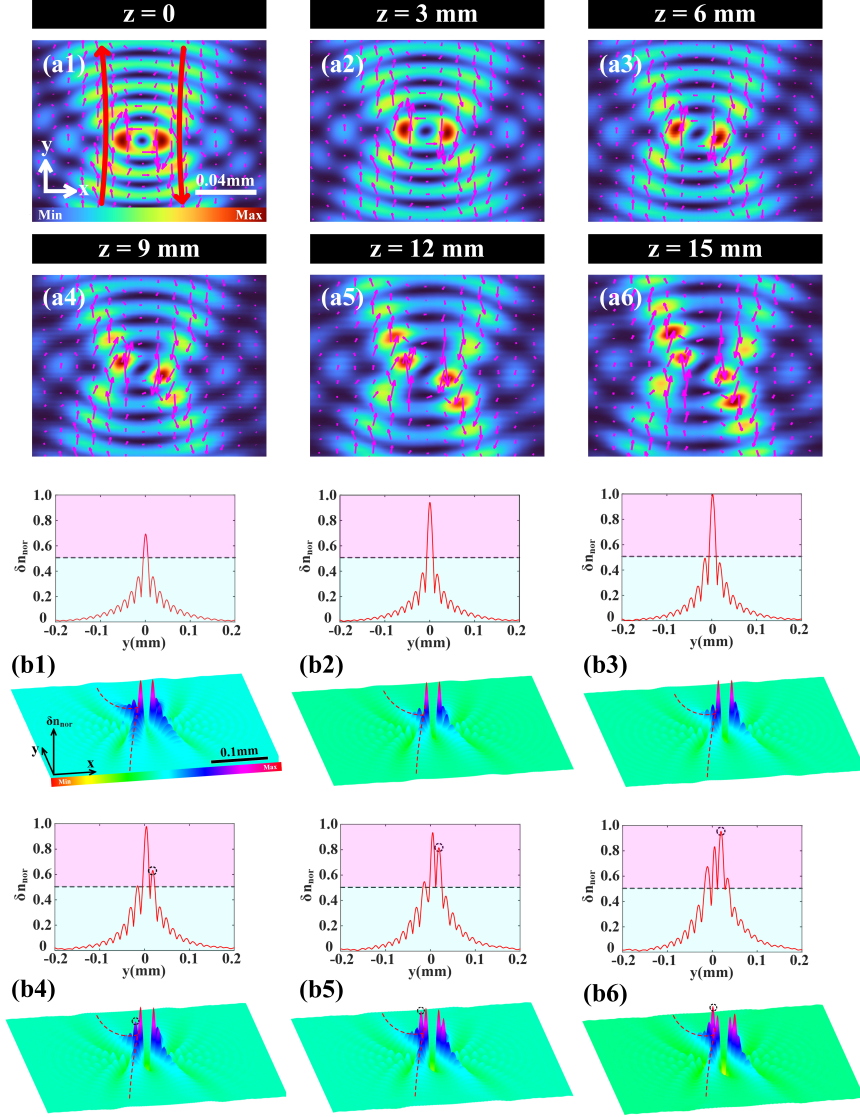


Figure 3: The explanation of the self-splitting. (a1)-(a6) The energy density of the NLGB and Poynting-vector patterns for different propagation distances. (b1)-(b6) Upper rows: The normalized refractive-index modulation along the left side of the main lobe, marked by the red dashed line in the lower rows (the picture is normalized by the maximum value of the refractive-index change, $\delta n_{\max} = 2.29 \times 10^{-4}$). Pink and blue shaded regions designate the normalized values which are higher and lower than 0.5, respectively, separated by the black dashed line. Lower rows: the three-dimensional visualization of the refractive index modulation, corresponding to (a1)-(a6).

demonstration of the positive feedback mechanism.

While direct experimental observation of internal profiles of the propagating beams is unfeasible, numerical simulations make it possible to monitor the dynamics inside the SBN crystal. Accordingly, in Fig. 4, we display the simulated evolution of the MLGB cross sections for different values of the splitting parameter x_0 and a fixed input power, $P = 4P_0$. Due to the applied additional spatial phase modulation, the MLGB splits in the transverse direction, from the middle towards both edges. The nonlinear dynamics is essentially the same as explored above. However, the comparison of Figs. 4 and 2(f) demonstrates that the splitting degree rises under the action of the spatial phase modulation added to the NLGB. The separation between the two high-energy stripes keeps increasing as x_0 rises and the stripes shift sideways. Our experimental results presented in the far right column of Fig. 4 verify the prediction.

It is relevant to consider potential applications of the self-splitting effect reported in this work. The SBN crystal, due to its unique ability to keep the memory of the refractive-index changes and the easy-to-erase property at relatively low writing laser powers [46], is an ideal platform for writing flexible and reconfigurable waveguides, which was reported in the investigation of spatial rotating solitons in Ref. [47]. To develop this possibility, we suppress the side lobes of the MLGB in Fig. 4(b) and set $n = 4$ in Eq. (1), to retain the input's central ring. As shown in Figs. 5(a1)-5(a6), the OAM-carrying MLGB initially undergoes splitting, with separating energy-density maxima. Then, two emerging main lobes rotate clockwise, realizing an effectively chiral waveguide. Further, after passing about 9 mm, the MLGB loses its vorticity, demonstrating solely diffraction with increasing separation between the main lobes. To provide an explanation of this behavior, we recall that, according to the Noether's theorem [48, 49], the angular momentum is not conserved if the system's rotational symmetry is broken (of course, the full angular momentum of the optical field and underlying material medium is conserved). In the underlying Eq. (5), the symmetry is obviously broken by the anisotropic term with $\partial/\partial x$. Indeed, the OAM-carrying MLGB rotates by a small angle in Figs. 5(a1)-5(a3) and

subsequently loses the vorticity in Figs. 5(a4)-5(a6). This argument explains the partial rotation of the incident beams under the action of the nonlinearity, resembling the effect of the optical field modulation in the free space [50, 51]. Alternatively, chiral waveguides may serve as an optical circular-dichroism device [52]. By simulating the phase evolution of the above-mentioned MLGB inside the SBN crystal, due to the inherent phase singularities defined by the OAM quantum number n , we notice the formation of a vortex with order 4, in Fig. 5(c6), which matches the number of side lobes at the output face of the SBN crystal in Fig. 5(a6). Further, we simulate the MLGB with $n = 2, 6, 8$ in Figs. 5(d1)-(f2), and conclude that the matching of side lobes and phase singularities is a result of imprinting the OAM vorticity (topological charge) from the phase pattern onto the density one. In other words, by counting the number of side lobes in the output, one can readily restore the topological charge carried by beam. Due to the degeneracy of adjacent odd and even topological charges, we here consider only vortices of even orders. These results can be used for the design of schemes for nonlinear coding and decoding in optical communications, cf. Refs. [53, 54].

4. Conclusion

In this work we have investigated, theoretically and experimentally, the propagation of nondiffractive beams in the photorefractive medium. The energy flow is visualized by the Poynting-vector field. The light-matter interaction gives rise to the self-splitting of the beams into separating secondary ones. The splitting degree is effectively controlled by means of the phase-pre-modulation method. We have also considered potential applications of the self-splitting for the design of an effectively chiral waveguide, using the memory feature of the photorefractive crystal. The nonlinear generation and characterization of vortices with even topological charges via output intensity pattern are considered too.

The results are reported in this paper for the self-focusing photorefractive nonlinearity. We have also performed experiments and simulations for the sys-

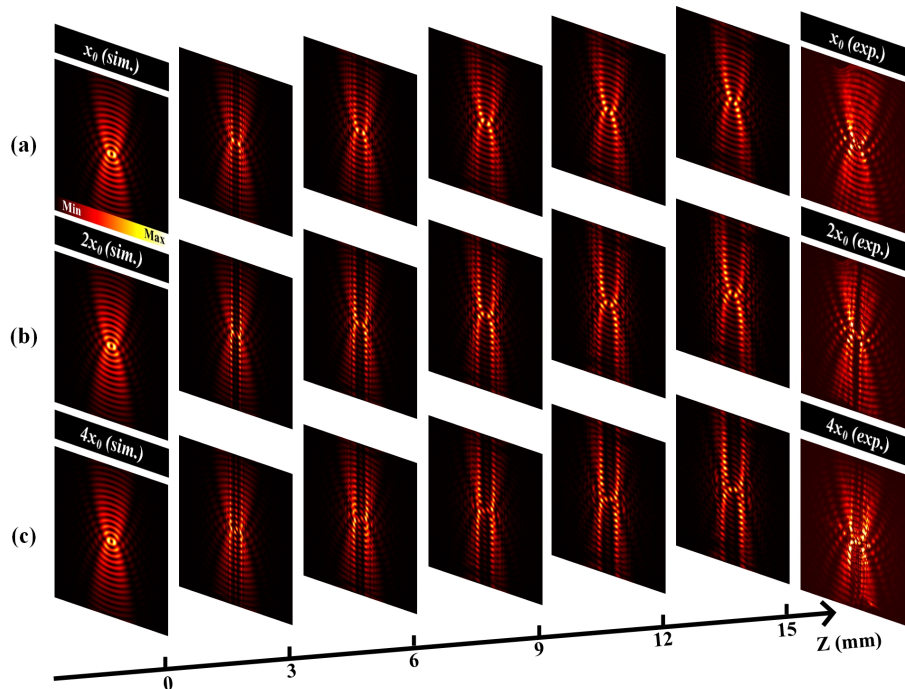


Figure 4: Cross sections of MLGBs produced by simulations of their propagation in the nonlinear medium, with different values of splitting parameter x_s and fixed $x_0 = 0.002$ mm. (a) $x_s = x_0$; (b) $x_s = 2x_0$; (c) $x_s = 4x_0$. The cross sections experimentally observed at the output face of the crystal are displayed in the far right column.

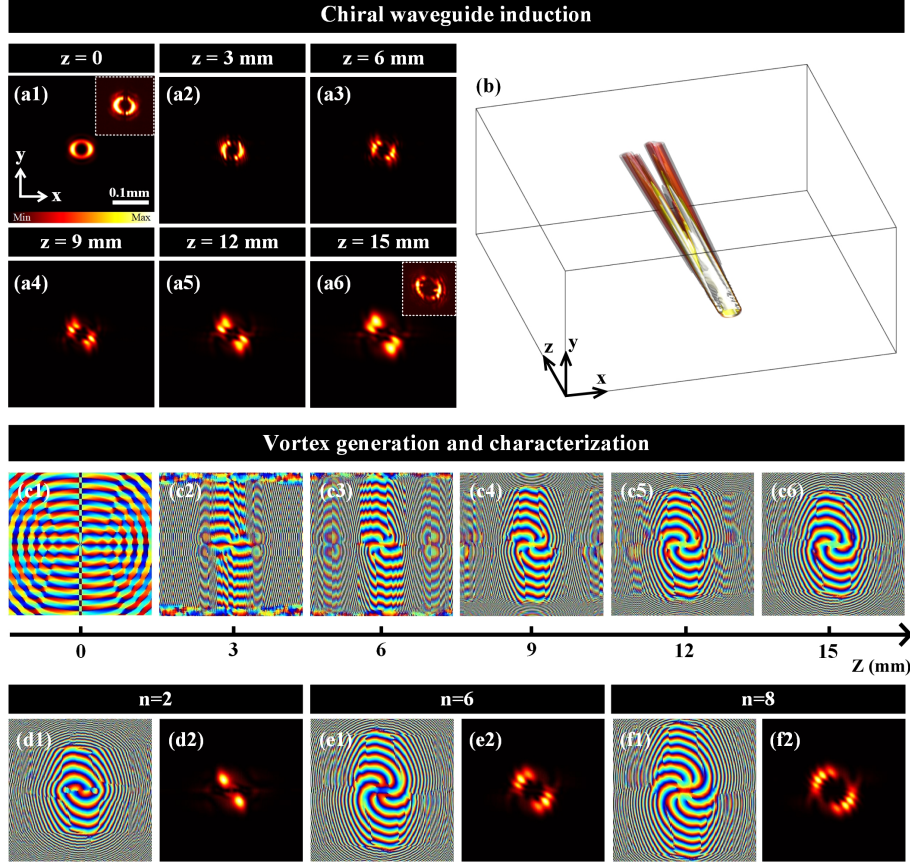


Figure 5: The demonstration of the nonlinearity-induced chiral waveguide and vortex generation. For the realization of the chiral waveguide induction, the input MLGB is taken as in Fig. 4(b), but with $n = 4$ in Eq. (1). The MLGB with pruned side lobes splits and rotates in the course of the propagation. Panels (a1)-(a6) display cross sections at different distances, as produced by the simulations. Insets in (a1) and (a6) show the corresponding experimental snapshots. (b) The simulated three-dimensional envelope of the self-splitting beam. Parameters of the MLGBs are $x_s = 2x_0$, $w_0 = a = 30 \mu\text{m}$ and $n = 4$, see Eq. (1). The bottom half of the figure demonstrates the generation and characterization of the vortex under the action of the nonlinearity. (c1)-(c6) The vortex formation with OAM order (topological charge) = 4. (d1)-(f2) Simulated vortex phase and intensity distributions with topological charges 2, 6 and 8, respectively.

tem with the self-defocusing sign. These results are not presented here, as they do not exhibit remarkable effects – in particular, no splitting is induced by the self-defocusing.

The experimental and theoretical work can be developed further. In particular, it may be relevant to consider interactions of two or several copropagating nondiffractive beams, including a possibility of formation of their (quasi-) bound states.

Acknowledgement

National Natural Science Foundation of China (12174122 and 11775083); Guangdong provincial Natural Science Foundation of China (Grant No. 2022A1515011482); Science and Technology Program of Guangzhou (No. 2019050001); Program of innovation and entrepreneurship for undergraduates; special funds for the cultivation of Guangdong college students scientific and technological innovation (Climbing Program special funds) (pdjh2022a0129, pdjh2023a0136); the Extracurricular Scientific Program of School of Information and Optoelectronic Science and Engineering, South China Normal University (22GDKB02); Israel Science Foundation (grant No. 1695/22).

Disclosures

The authors declare no conflicts of interest.

Data availability

Data underlying the results presented in this paper are not publicly available at this time but may be obtained from the authors upon reasonable request.

References

- [1] J. Shalf, The future of computing beyond moore’s law, *Philosophical Transactions of the Royal Society A* 378 (2166) (2020) 20190061.

- [2] G. Chen, N. Li, J. D. Ng, H.-L. Lin, Y. Zhou, Y. H. Fu, L. Y. T. Lee, Y. Yu, A.-Q. Liu, A. J. Danner, Advances in lithium niobate photonics: development status and perspectives, *Advanced Photonics* 4 (3) (2022) 034003–034003.
- [3] M. Li, J. Ling, Y. He, U. A. Javid, S. Xue, Q. Lin, Lithium niobate photonic-crystal electro-optic modulator, *Nature Communications* 11 (1) (2020) 4123.
- [4] Q. Zhao, W. Yuan, J. Qu, Z. Cheng, G.-D. Peng, C. Yu, Optical fiber-integrated metasurfaces: An emerging platform for multiple optical applications, *Nanomaterials* 12 (5) (2022) 793.
- [5] J. D. Joannopoulos, P. R. Villeneuve, S. Fan, Photonic crystals, *Solid State Communications* 102 (2-3) (1997) 165–173.
- [6] R. K. Cersonsky, J. Antonaglia, B. D. Dice, S. C. Glotzer, The diversity of three-dimensional photonic crystals, *Nature communications* 12 (1) (2021) 2543.
- [7] J. Valentine, S. Zhang, T. Zentgraf, E. Ulin-Avila, D. A. Genov, G. Bartal, X. Zhang, Three-dimensional optical metamaterial with a negative refractive index, *nature* 455 (7211) (2008) 376–379.
- [8] K. Koshelev, A. Bogdanov, Y. Kivshar, Meta-optics and bound states in the continuum, *Science Bulletin* 64 (12) (2019) 836–842.
- [9] S. Coe-Sullivan, Quantum dot developments, *Nature Photonics* 3 (6) (2009) 315–316.
- [10] Y.-S. Park, J. Roh, B. T. Diroll, R. D. Schaller, V. I. Klimov, Colloidal quantum dot lasers, *Nature Reviews Materials* 6 (5) (2021) 382–401.
- [11] C. Wang, M. Zhang, B. Stern, M. Lipson, M. Lončar, Nanophotonic lithium niobate electro-optic modulators, *Optics express* 26 (2) (2018) 1547–1555.

- [12] T. Ozawa, H. M. Price, A. Amo, N. Goldman, M. Hafezi, L. Lu, M. C. Rechtsman, D. Schuster, J. Simon, O. Zilberberg, et al., Topological photonics, *Reviews of Modern Physics* 91 (1) (2019) 015006.
- [13] M. Kim, Z. Jacob, J. Rho, Recent advances in 2d, 3d and higher-order topological photonics, *Light: Science & Applications* 9 (1) (2020) 130.
- [14] M. Segev, M. A. Bandres, Topological photonics: Where do we go from here?, *Nanophotonics* 10 (1) (2020) 425–434.
- [15] Y.-R. Shen, *Principles of nonlinear optics*, Wiley-Interscience, New York, NY, USA, 1984.
- [16] C. Cui, L. Zhang, L. Fan, In situ control of effective kerr nonlinearity with pockels integrated photonics, *Nature Physics* 18 (5) (2022) 497–501.
- [17] T. Omatsu, N. M. Litchinitser, E. Brasselet, R. Morita, J. Wang, Focus issue introduction: synergy of structured light and structured materials, *Optics Express* 25 (14) (2017) 16681–16685.
- [18] A. Ashkin, G. Boyd, J. i. Dziedzic, R. Smith, A. Ballman, J. Levinstein, K. Nassau, Optically-induced refractive index inhomogeneities in LiNbO_3 and LiTaO_3 , *Applied Physics Letters* 9 (1) (1966) 72–74.
- [19] B. Terhalle, *Controlling light in optically induced photonic lattices*, Springer Science & Business Media, 2011.
- [20] N. Kukhtarev, V. Markov, S. Odulov, M. Soskin, V. Vinetskii, Holographic storage in electrooptic crystals. i. steady state, *ferroelectrics* 22 (1) (1978) 949–960.
- [21] S. Liu, Y. Hu, P. Zhang, X. Gan, F. Xiao, C. Lou, D. Song, J. Zhao, J. Xu, Z. Chen, Anomalous interactions of spatial gap solitons in optically induced photonic lattices, *Optics letters* 36 (7) (2011) 1167–1169.
- [22] S. Xia, D. Jukić, N. Wang, D. Smirnova, L. Smirnov, L. Tang, D. Song, A. Szameit, D. Leykam, J. Xu, et al., Nontrivial coupling of light into a

- defect: the interplay of nonlinearity and topology, *Light: Science & Applications* 9 (1) (2020) 147.
- [23] J. W. Fleischer, T. Carmon, M. Segev, N. K. Efremidis, D. N. Christodoulides, Observation of discrete solitons in optically induced real time waveguide arrays, *Physical review letters* 90 (2) (2003) 023902.
- [24] P. Rose, F. Diebel, M. Boguslawski, C. Denz, Airy beam induced optical routing, *Applied Physics Letters* 102 (10) (2013).
- [25] A. Zannotti, J. M. Vasiljević, D. V. Timotijević, D. M. Jović Savić, C. Denz, Visualizing the energy flow of tailored light, *Advanced Optical Materials* 6 (8) (2018) 1701355.
- [26] A. Zannotti, J. M. Vasiljević, D. V. Timotijević, D. M. J. Savić, C. Denz, Morphing discrete diffraction in nonlinear mathieu lattices, *Optics Letters* 44 (7) (2019) 1592–1595.
- [27] W. Ma, Y. Zhuang, Z. Wang, P. Jia, P. Zhang, Y. Hu, Z. Chen, J. Xu, Breaking the action-reaction principle of light interactions under a stroboscopic nonlinearity, *Laser & Photonics Reviews* 17 (2) (2023) 2200177.
- [28] S. Xia, D. Kaltsas, D. Song, I. Komis, J. Xu, A. Szameit, H. Buljan, K. G. Makris, Z. Chen, Nonlinear tuning of pt symmetry and non-hermitian topological states, *Science* 372 (6537) (2021) 72–76.
- [29] F. Diebel, P. Rose, M. Boguslawski, C. Denz, Observation of spatially oscillating solitons in photonic lattices, *New Journal of Physics* 18 (5) (2016) 053038.
- [30] J. Armijo, R. Allio, Observation of coherent back-scattering and its dynamics in a transverse 2d photonic disorder: from weak to strong localization, *arXiv preprint arXiv:1504.07340* (2015).
- [31] T. Schwartz, G. Bartal, S. Fishman, M. Segev, Transport and anderson localization in disordered two-dimensional photonic lattices, *Nature* 446 (7131) (2007) 52–55.

- [32] I. Julián-Macías, C. Rickenstorff-Parrao, O. de Jesús Cabrera-Rosas, E. Espíndola-Ramos, S. A. Juárez-Reyes, P. Ortega-Vidals, G. Silva-Ortigoza, C. T. Sosa-Sánchez, Wavefronts and caustics associated with mathieu beams, *JOSA A* 35 (2) (2018) 267–274.
- [33] Y. Shen, S. Pidishety, I. Nape, A. Dudley, Self-healing of structured light: a review, *Journal of Optics* 24 (10) (2022) 103001.
- [34] S. Li, J. Wang, Adaptive free-space optical communications through turbulence using self-healing bessel beams, *Scientific reports* 7 (1) (2017) 43233.
- [35] T. U. Tumkur, T. Voisin, R. Shi, P. J. Depond, T. T. Roehling, S. Wu, M. F. Crumb, J. D. Roehling, G. Guss, S. A. Khairallah, et al., Nondiffractive beam shaping for enhanced optothermal control in metal additive manufacturing, *Science Advances* 7 (38) (2021) eabg9358.
- [36] F. Diebel, M. Boguslawski, T. Dadalyan, R. Drampyan, C. Denz, Controlled soliton formation in tailored bessel photonic lattices, *Optics Express* 24 (12) (2016) 12933–12940.
- [37] C. Michel, O. Boughdad, M. Albert, P.-É. Larré, M. Bellec, Superfluid motion and drag-force cancellation in a fluid of light, *Nature communications* 9 (1) (2018) 2108.
- [38] A. A. Kovalev, V. V. Kotlyar, Family of three-dimensional asymmetric nonparaxial lommel modes, in: *Saratov Fall Meeting 2014: Optical Technologies in Biophysics and Medicine XVI; Laser Physics and Photonics XVI; and Computational Biophysics*, Vol. 9448, SPIE, 2015, pp. 565–571.
- [39] S. Edition, *Table of integrals, series, and products*, Elsevier, 2007.
- [40] G. P. Agrawal, Nonlinear fiber optics, in: *Nonlinear Science at the Dawn of the 21st Century*, Springer, 2000, pp. 195–211.
- [41] A. A. Zozulya, D. Z. Anderson, Propagation of an optical beam in a photorefractive medium in the presence of a photogalvanic nonlinearity or an externally applied electric field, *Physical Review A* 51 (2) (1995) 1520.

- [42] L. Allen, M. Padgett, M. Babiker, Iv the orbital angular momentum of light, in: *Progress in optics*, Vol. 39, Elsevier, 1999, pp. 291–372.
- [43] A. Zannotti, F. Diebel, M. Boguslawski, C. Denz, Chiral light in helically twisted photonic lattices, *Advanced Optical Materials* 5 (16) (2017) 1600629.
- [44] P. Yeh, W. Moerner, *Introduction to photorefractive nonlinear optics* (1994).
- [45] O. Boughdad, A. Eloy, F. Mortessagne, M. Bellec, C. Michel, Anisotropic nonlinear refractive index measurement of a photorefractive crystal via spatial self-phase modulation, *Optics express* 27 (21) (2019) 30360–30370.
- [46] S. Xia, A. Ramachandran, S. Xia, D. Li, X. Liu, L. Tang, Y. Hu, D. Song, J. Xu, D. Leykam, et al., Unconventional flatband line states in photonic lieb lattices, *Physical review letters* 121 (26) (2018) 263902.
- [47] T. Carmon, R. Uzdin, C. Pigier, Z. H. Musslimani, M. Segev, A. Nepomnyashchy, Rotating propeller solitons, *Physical Review Letters* 87 (14) (2001) 143901.
- [48] M. Safdar, A. Qadir, M. U. Farooq, Comparison of noether symmetries and first integrals of two-dimensional systems of second order ordinary differential equations by real and complex methods, *Symmetry* 11 (9) (2019) 1180.
- [49] Y. Kosmann-Schwarzbach, B. E. Schwarzbach, Y. Kosmann-Schwarzbach, *The noether theorems*, Springer, 2011.
- [50] Z. Liang, J. Shi, Q. Wei, Z. Wang, Y. Wu, J. Jiang, L. Shui, D. Deng, Asymmetrical inseparable coherent structures, *Optics Letters* 47 (10) (2022) 2426–2429.
- [51] L. Wan, D. Zhao, Controllable rotating gaussian schell-model beams, *Optics Letters* 44 (4) (2019) 735–738.

- [52] T. Shi, Z.-L. Deng, G. Geng, X. Zeng, Y. Zeng, G. Hu, A. Overvig, J. Li, C.-W. Qiu, A. Alù, et al., Planar chiral metasurfaces with maximal and tunable chiroptical response driven by bound states in the continuum, *Nature Communications* 13 (1) (2022) 4111.
- [53] A. E. Willner, K. Pang, H. Song, K. Zou, H. Zhou, Orbital angular momentum of light for communications, *Applied Physics Reviews* 8 (4) (2021).
- [54] Y. Shen, X. Wang, Z. Xie, C. Min, X. Fu, Q. Liu, M. Gong, X. Yuan, Optical vortices 30 years on: Oam manipulation from topological charge to multiple singularities, *Light: Science & Applications* 8 (1) (2019) 90.